Applied Mathematical Modelling 52 (2017) 648–663

Contents lists available at ScienceDirect

Applied Mathematical Modelling

journal homepage: www.elsevier.com/locate/apm

A hybrid analytical-numerical method for solving water flow equations in root hydraulic architectures

Félicien Meunier[a,*], Xavier Draye[b], Jan Vanderborght[c,d], Mathieu Javaux[a,d], Valentin Couvreur[b]

[a] Earth and Life Institute-Environnement, Université catholique de Louvain, Belgium
[b] Earth and Life Institute-Agronomy, Université catholique de Louvain, Belgium
[c] Division of soil and water management, Katholieke Universiteit Leuven, Belgium
[d] Forschungszentrum Juelich GmbH, Agrosphere Institute, IBG-3, Juelich, Germany

ARTICLE INFO

Article history:
Received 12 January 2017
Revised 28 July 2017
Accepted 3 August 2017
Available online 14 August 2017

Keywords:
Root system hydraulic architecture
Segment-scale analytical solution
Water flow equation
Root water uptake

ABSTRACT

In this manuscript, we propose a new method to calculate water flow and xylem water potential distribution in hydraulic architectures (such as root systems) of any complexity. It is based on the extension of the water flow equation analytical resolution of Landsberg and Fowkes for single roots. It consists in splitting the root systems in zones of homogeneous or homogeneously changing properties and deriving the xylem potential and water flow under any given boundary conditions (plant transpiration or collar potential, and potential at soil-root interfaces) without assuming a uniform xylem potential within each zone. The method combines analytical solutions of water flow within the segmented zones with the numerical solution of flow connectivity for the whole root system.

We demonstrate that the proposed solution is the asymptote of the exclusively numerical solution for infinitesimal root segment lengths (and infinite segment number). As water uptake locations and magnitudes predicted by the latter solution for finite segmentation lengths deviate from the exact solution, and are computationally more intensive, we conclude that the new methodology should always be privileged for future applications.

The proposed solution can be easily coupled to soil modules (as already done with existing solutions) and further implemented in functional-structural plant models to predict water flow in the soil-plant atmosphere continuum with a better accuracy than current models. Finally the new solution may be used to calculate more accurately plant scale macroscopic parameters for crop models.

1. Introduction

Ensuring crop productivity under conditions of long term change of soil water availability and atmospheric demand for water requires a thorough understanding of crop bio-physical properties to acquire soil water [1]. Even though simple

Abbreviations: PLT, Stand for pressure, length and time units respectively; HA, Hydraulic architecture; RS, Root system; CPU, central processing unit; RWU, root water uptake; RSHA, Root system hydraulic architecture.

* Corresponding author.
E-mail address: felicien.meunier@uclouvain.be (F. Meunier).

http://dx.doi.org/10.1016/j.apm.2017.08.011
0307-904X/

empirical models of crop transpiration benefit from consequent parameter libraries [2], they may lose their predictive power under changing conditions, such as changing soil type or soil water content distribution [3–5]. Bio-physical principles, such as water flow dynamics, integrated in crop water acquisition models might better address questions of water availability for future crop-climate combinations.

Root system water uptake and flow can be represented via a system of equations representing radial (between soil-root interfaces to xylem) and axial (within the xylem network) flow equations analogous to Ohm law [6]. Axial law within xylem has been demonstrated to be similar to Poiseuille law [7]. Radial water flow is known to be extremely complex due to the coexistence of several flow pathways but the ohm analogy has been shown to be relevant [8]. Mass conservation allows one to link radial and axial flow equations, which can then be solved analytically for single roots with or without laterals [9,10]. Analytical solutions for complete root system have also been developed [11,12] but they are based on several simplifying assumptions (as no pressure loss in the lateral roots, a simplified root architecture etc.).

In addition, numerical solutions have been developed to solve more complex root system hydraulic architecture [13]. In 1998, Doussan et al. [14] proposed a model for solving water flow in a xylem network of a root system of any complexity as a function of the soil hydraulic status for any xylem collar boundary conditions (flux or potential). The root system architecture must first be split into small parts called segments of homogeneous hydraulic properties (i.e., radial and axial conductivity) and their connections (i.e., the root system architectural properties) are gathered in an incidence matrix. The model splits the water transfer from the soil-root interface in a radial pathway (driven by segment radial conductivity, mainly characterized by the Casparian strip) and an axial movement (driven by xylem vessels ability to transport the water, quantified by the segment axial conductivity). Assuming a constant potential in the xylem vessels of the segment a set of linear equations can be solved to obtain the radial flow and the xylem potential in any position of the root system according to overall boundary conditions: plant collar water flux or potential, and water potential at soil-root interfaces [14] For further description of model assumptions and included processes, we refer to the original publication [14].

Methods for solving the water flow equations in hydraulic architectures have been used for many applications from inverse parametrization [15] to prediction [7] and process understanding [16]. The model was considered alone [14] or coupled to soil models (i.e., to simulate dynamic root water uptake and water transfer in three-dimensional soil-root continuum under changing atmospheric conditions, see for example [17]).

However the assumption of a constant potential inside a root segment is not valid: the hydraulic potential cannot be uniform in a root portion of finite length (the water movement would then be null within the segment). The resulting errors can be reduced by dividing the root system in smaller and smaller root segments but rapidly the computational time to solve the water flow inside the root system becomes limiting. As a consequence a compromise must be made between accuracy and efficiency.

More sophisticated models of water flow across unbranched roots account for root anatomy and hydraulic properties of cell walls and membranes in each root tissue (see for example [18–20]) These models have proven their value for questions of solute transport across roots ([21,22]). As far as water is concerned, the simpler root cylinder model [8] used here for radial flow was experimentally demonstrated to be satisfying (see review [23]). Furthermore, recent modeling work on radial water flow across explicit maize root cross-sections demonstrated that the root cylinder model is equivalent to the detailed hydraulic anatomical approach [24], regardless of the level of apoplastic barrier leakiness.

More detailed models of the root radial water flow (such as the one developed by Claus et al. [22] or Foster and Miklavcic [25]) could be used in the future to better parametrize the root radial hydraulic properties based on cell level properties.

All the models of root systems are flawed because of the segment constant potential assumption. One particular application of Doussan et al. model was to identify and calculate emergent plant scale hydraulic properties (or “macroscopic” hydraulic parameters) from root system architecture and local root hydraulic properties [26]. Existing methods for calculating these macroscopic parameters have therefore the same limited accuracy as Doussan et al. model [14].

The objective of this study is to provide a new resolution of the water flow equations in a root system hydraulic architecture (RSHA) with better accuracy than existing methods. To do so, we implemented an analytical solution of the water flow at the root segment scale in a connection matrix representing the root system architecture. The central idea is thus to work at two different levels: (1) at the plant root level, the root system (RS) architecture is divided into segments small enough to keep the features of the architecture, but potentially larger than in typical finite difference approaches and, (2) at the root segment level where an analytical solution is used to describe water flow. The new hybrid solution therefore does not require infinite refining of the root system to get closer to the exact water flow in the RSHA. Both methodologies can be compared in terms of computer efficiency and accuracy. The hybrid (or combined) approach allows the calculation of the macroscopic parameters of RSHA more accurately and more quickly for using the Couvreur et al. model [26].

In this paper, we first detail the finite-difference method of Doussan et al. [14] hereafter referred alternatively to as the “Doussan model” or the “finite-difference approach”, for solving the water flow in a RSHA (Section 2.1.1) and the upscaled model of Couvreur et al. [26], hereafter referred to as the “Couvreur model”, for calculating the macroscopic parameters (Section 2.1.2). We then develop the new resolution method of the water flow (Section 2.2) using the analytical solution at the segment scale [9] which has been extended by Meunier et al. [10] (Section 2.1.3) We refer to the new solution alternatively to as the hybrid or the combined approach. Finally, we illustrate the benefits of using such a methodology as compared with existing methods in terms of accuracy and efficiency with five different tests mixing numerical simulations and experimental data (Sections 3 and 4).

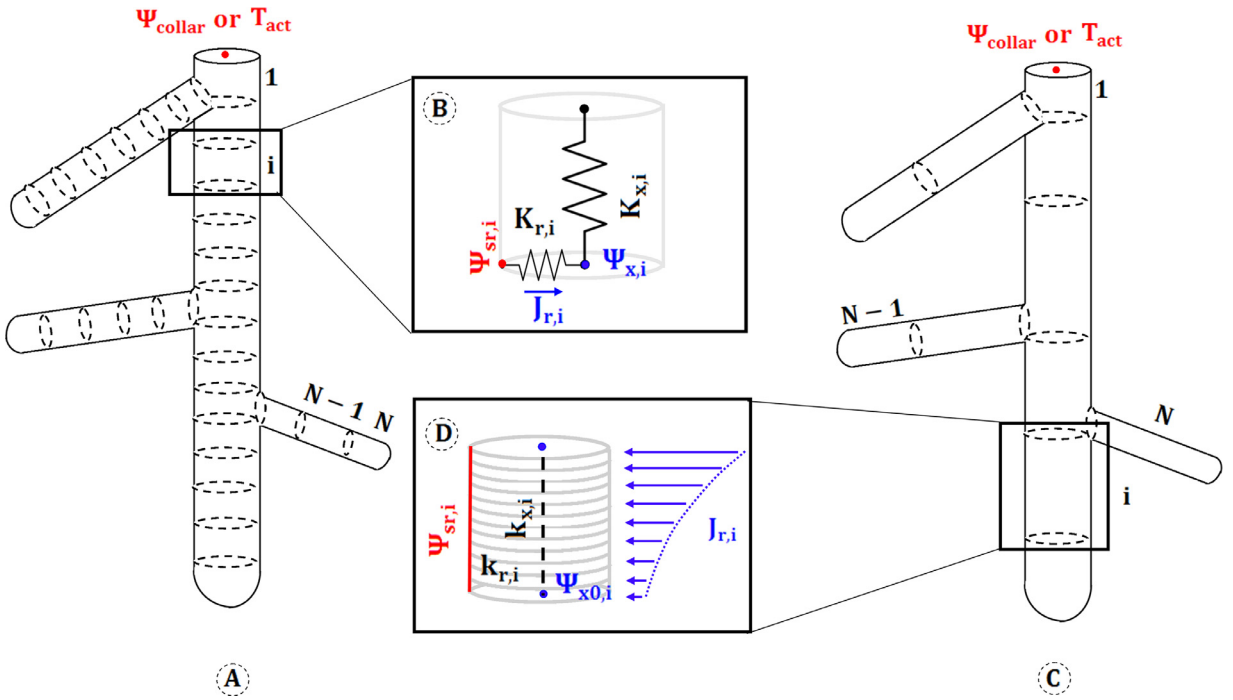

Fig. 1. (A) Schematic of a simple root system made of 30 segments (N = 30) with (B) a zoom-in on a particular segment (numbered i). Each single segment is characterized by a radial conductance K_r and an axial conductance K_x. When the boundary conditions are provided (indicated here in red), water flow equations can be solved and lead to the xylem potential and radial flow distribution in the root system, solutions of the water flow equation. (C) Schematic of the same root system cut in 11 homogeneous (or homogeneously changing) zones (N = 11) with (D) a zoom-in on a particular root zone numbered i and characterized by inherent radial conductivity and axial hydraulic conductance k_r and k_x. Again, the boundary conditions lead to the solution of the problem: the distal xylem potential and the proximal axial flow. (For interpretation of the references to colour in this figure legend, the reader is referred to the web version of this article.)

2. Theory

2.1. Existing approaches for modeling water flow dynamics in hydraulic architectures

In this section, three existing models of water flow are presented, whose description is relevant before further developing equations of the new model. The description is rather detailed in order to allow a final parallel comparison of the coefficients of each model and to clearly link their respective parameters. In this manuscript, we note the vectors and matrices as bold. We indicate the dimensions of the vectors and matrices between square brackets and units between regular parentheses.

2.1.1. Finite-difference solution of water flow in root systems

The finite-difference approach is part of van den Honert's lineage of physical models [27] based on Ohm's analogy to describe water flow in plants [9,17,28–30] of any complexity. However, for the first time, they proposed a matrix operation to solve water flow in three-dimensional HAs of any complexity.

Considering a root system made of root segments numbered from 1 to N, a vector $\mathbf{K_x}$ [N × 1] contains root segments axial conductances ($L^3\ P^{-1}\ T^{-1}$, see abbreviation section for unit description), for axial water flow towards the upper root segment in xylem ($K_{x,1}$) being the axial conductance between the first root segment and plant collar, where a water flow, or water potential, boundary condition is imposed). A second vector $\mathbf{K_r}$ [N × 1] contains root segments radial conductances ($L^3\ P^{-1}\ T^{-1}$), for water flow between soil-root interface and root xylem. For each root segment, total water potential (P) (which is the sum of matric and gravitational potentials) is defined in root xylem and at soil-root interface and contained respectively in vectors $\mathbf{\Psi_x}$ [N × 1] and $\mathbf{\Psi_{sr}}$ [N × 1]. Note that both $\mathbf{K_x}$ and $\mathbf{K_r}$ depend on the segment size: they are not intrinsic properties of the root tissues [17]. Note also that conductance and water potential units differ from the standard usage in soil physics (where $L^2\ T^{-1}$ and L are more commonly used): we use here water potential per volume rather than water head (water potential per weight) for consistency with plant physiology common units. Note also that our definition of the water potential includes the gravity, which allows the model to simulate water flow in non-horizontal roots (and potentially in three-dimensional root systems).

An example of simple root system is represented in Fig. 1a. It is made of a main root and three laterals and divided into 30 root segments numbered from 1 to N. The frame (Fig. 1b) zooms in on a particular segment i characterized by radial (K_r) and axial (K_x) conductances, which we indicate by the subscript i.

By rearranging the system of mass conservation equations, Doussan et al. provided the following expression of xylem water potential under flux-type boundary condition [6]:

$$\begin{bmatrix} \Psi_{collar} \\ \mathbf{\Psi_x} \end{bmatrix} = \mathbf{C}^{-1}.\mathbf{D} \quad (1)$$

where Ψ_{collar} (P) is the plant collar water potential, $\mathbf{D}$ [N + 1 × 1] contains T_{act} (L^3T^{-1}), the plant actual transpiration as imposed at plant collar, and $\mathbf{C}^{-1}$ [N + 1 × N + 1] is the inverse of $\mathbf{C}$ matrix of conductances. The detailed procedure to build $\mathbf{C}$ and $\mathbf{D}$ is described in Appendix A.

Under water potential-type boundary condition at plant collar, the expression for $\mathbf{\Psi_x}$ becomes:

$$\mathbf{\Psi_x} = \mathbf{c}^{-1}.\,\mathbf{d} \quad (2)$$

Again the matrix $\mathbf{d}$ [N × 1] contains the top boundary conditions, the imposed collar potential Ψ_{collar} and $\mathbf{c}^{-1}$ is the inverse of $\mathbf{c}$, the reduced conductance matrix. Appendix A also details how to build $\mathbf{c}$ and $\mathbf{d}$.

Under both boundary condition types, equations of potential-driven water flow (Ohm's analogue) allow calculating RWU rates $\mathbf{J_r}$ ($L^3\ T^{-1}$) [N × 1] at soil-root interfaces (positive from soil-root interfaces towards the xylem vessels):

$$\mathbf{J_r} = \mathbf{diag}(\mathbf{K_r}).\ (\mathbf{\Psi_{sr}} - \mathbf{\Psi_x}) \quad (3)$$

In the next pages, Eqs. (1)–(3) will be referred to as "Doussan equations" and the method to solve the water flow problem as the "Doussan model" or the "finite-difference approach".

In Fig. 1a and b, when the boundary conditions (in red) are known (i.e., soil-root interface potential and collar flow or potential), root system variables (in blue) can be calculated using the Doussan model. The solution of the water flow equation in roots is instantaneous (as long as there is no hydraulic capacity considered, as it is here) but the solution can be applied for transient boundary conditions as long as small time steps that follow the boundary condition dynamics are used.

The Doussan model has the advantage to allow representing the complexity of RS architectures at a scale at which hydraulic parameters can be measured. Root system architecture information is contained in the **IM** matrix, which can either be built (i) using new or ancient techniques, destructive or not, to scan experimental RS [15,32–36], or (ii) using softwares to generate virtual RS architectures [37,38] based on information on root types, densities, branching and growth rates available in the literature, as carried out for maize, wheat and ryegrass and others (see for example [26,39] and [40]). The emergence of a common format for storing root system architectures (i.e., RSML for root system markup language) opens new avenues for the plant and soil scientific community to share architectural information obtained from experiments to numerical models [41].

Information on root hydraulic properties is contained in vectors $\mathbf{K_x}$ and $\mathbf{K_r}$. They can either be (i) measured with direct techniques such as developed by Sanderson et al. [42] and Frensch and Steudle [43], (ii) estimated from flux measurements via inverse modeling [15] or (iii) taken from the literature, in which typical radial and axial root conductances are related to root age and type [31,44,45].

2.1.2. Macroscopic hydraulic architecture approach

Following Doussan model's basic assumptions, the Couvreur model provides a direct solution of water flow in root system HA of any complexity based on macroscopic parameters. This study uses the root system form of this model to stay consistent with the finite-difference approach.

The expression for RWU by individual root segments is the following:

$$\mathbf{J_r} = T_{act}\mathbf{SUF} + K_{comp}(\mathbf{\Psi_{sr}} - \Psi_{seq}) \odot \mathbf{SUF} \quad (4)$$

where $\mathbf{SUF}$ [N × 1](−) is the vector of standard uptake fractions of root segments, K_{comp} ($L^3\ P^{-1}\ T^{-1}$) is the compensatory RWU conductance of the plant, ⊙ indicates an Hadamard product and Ψ_{seq} (P) is the equivalent soil water potential sensed by the plant, which is a weighted-average of water potentials at soil-root interfaces: $\Psi_{seq} = \mathbf{SUF^t}.\mathbf{\Psi_{sr}}$.

In Eq. (4), the first term on the right-hand-side is interpreted as the "standard RWU", driven by plant actual transpiration, while the second term is interpreted as the "compensatory RWU", driven by water potential heterogeneity at soil-root interfaces. As compared to the Doussan model, basic equations are the same (mass conservation and water potential-driven water flow equations), but an additional assumption is required for the compensatory RWU term: axial resistances need to be negligible as compared to radial resistances to water flow. The parameter K_{comp} only exists when the latter assumption is fulfilled, which makes it the only "non-exact" parameter of the simple macroscopic approach of root system HA. If this assumption is not valid, the Couvreur approach can also be used but with a more complex form for the second term of Eq. (4).

This approach also allowed to demonstrate the simple relationship linking Ψ_{seq}, Ψ_{collar} and T_{act}, which can be used to predict plant transpiration under water stress for isohydric plants:

$$T_{act} = K_{rs}\ (\Psi_{seq} - \Psi_{collar}) \quad (5)$$

where K_{rs} ($L^3\ P^{-1}\ T^{-1}$) is the equivalent conductance of the root system. In opposition to the compensatory RWU term of Eq. (4), this equation is an exact solution of Doussan set of equations.

The simplified macroscopic HA approach has the advantage to rely on few macroscopic parameters measurable and with physical meaning. Each of them contains information about both RS architecture and roots hydraulic conductances.

The numerical calculation of K_{rs} and **SUF** can be achieved by solving Eqs. (1) or (2) and (3) under conditions of uniform water potential at soil-root interfaces ($\boldsymbol{\Psi_{sr}} = \Psi_{seq}$), which provides Ψ_{collar} and $\mathbf{J_r}$ for Eqs. (4) and (5):

$$K_{rs} = \frac{T_{act}}{\Psi_{seq} - \Psi_{collar}} \tag{6}$$

$$\mathbf{SUF} = \frac{\mathbf{J_r}}{T_{act}} \tag{7}$$

The calculation of K_{comp} requires solving Eqs. (1) or (2) and (3) under conditions of heterogeneous water potential at soil-root interfaces. Then, K_{comp} can be estimated by linear regression using Eq. (4):

$$K_{comp} = \frac{(\boldsymbol{\Psi_{sr}} - \Psi_{seq})^t.(\mathbf{J_r} \oslash \mathbf{SUF} - T_{act})}{(\boldsymbol{\Psi_{sr}} - \Psi_{seq})^t.(\boldsymbol{\Psi_{sr}} - \Psi_{seq})} \tag{8}$$

Other parameterization methods exist. For instance K_{rs} can be calculated by using Thevenin theorem of equivalent conductances [46]. Experimental characterization of K_{rs} is also possible by using a water pressurisation technique and measuring outflow rate at plant collar [47,48]. Eventually, given the low number of parameters (**SUF** then being approximated by a simple function of space), inverse modeling could be envisaged to estimate their values.

However, a parameterization is valid for a given root system architecture and distribution of root hydraulic properties. If any of these features evolve with time, a new parameterization would be required anytime they would change.

2.1.3. Analytical solution of water flow in a homogeneous root stretch

In the following, we define a root zone as a root segment or a combination of root segments without lateral branches in which root properties are uniform (but not the root xylem potential). The exact solution of the water flow equation in a root cylinder of length $l_i(L)$ and radius $r_i(L)$ (the subscript i indicates the root zone) is given, according to Landsberg and Fowkes [9] by:

$$\Psi_{x,i}(z) = \Psi_{sr,i} + c_{1,i}\cosh(\tau_i z) + c_{2,i}\sinh(\tau_i z) \tag{9}$$

where $\Psi_{x,i}(P)$ is the xylem potential along the root axis, z (L) is the position along this axis (comprised between 0 and l_i), $\Psi_{sr,i}(P)$ is the soil-root interface potential supposed to be uniform, $c_{1,i}(P)$ and $c_{2,i}(P)$ are coefficients that depend on the boundary conditions and $\tau_i\,(L^{-1})$ is defined as:

$$\tau_i = \sqrt{\frac{2\pi r_i k_{r,i}}{k_{x,i}}}$$

with $k_{r,i}\,(L\,P^{-1}T^{-1})$ and $k_{x,i}\,(L^4\,P^{-1}T^{-1})$ the root radial conductivity and axial conductance, respectively. Both are inherent root tissue properties. The coefficients, $c_{1,i}$ and $c_{2,i}$, depend on boundary conditions applied on both sides of this root segment. Appendix B details their calculation under flux condition at the distal end, $J_{distal,i}(L^3T^{-1})$ and collar condition at the proximal end of the root segment, $\Psi_{proximal,i}\,(P)$. They then can be used to obtain the distal potential $\Psi_{x0,i}\,(P)$ and the proximal flow $J_{xl,i}\,(L^3T^{-1})$ of the root cylinder of uniform hydraulic properties called stretch i (see Appendix B for details on their calculation). It yields:

$$\Psi_{x0,i} = \Psi_{sr,i} + \frac{\Psi_{proximal,i} - \Psi_{sr,i} + \frac{J_{distal,i}}{\kappa_i}\sinh(\tau_i l_i)}{\cosh(\tau_i l_i)} \tag{10}$$

$$J_{xl,i} = \left(-\Psi_{proximal,i} + \Psi_{sr,i} - \frac{J_{distal,i}}{\kappa_i}\sinh(\tau_i l_i)\right)\kappa_i \tanh(\tau_i l_i) + J_{distal,i}\cosh(\tau_i l_i) \tag{11}$$

$$\text{with } \kappa_i = \sqrt{2\pi r_i k_{r,i} k_{x,i}}\ (L^3P^{-1}T^{-1})$$

Let us note that Eq. (9) can also be solved under a top flux $J_{proximal,i}\,(L^3\,T^{-1})$ boundary condition (imposed transpiration). Appendix C shows how it affects the coefficients $c_{1,i}$ and $c_{2,i}$. Other solutions when root hydraulic properties are not homogeneous also exist and can be used if desired [49].

2.2. Development of exact solutions

In this section, a new solution of water flow equations in RSHA is developed, where the simplifying assumption of constant water potential inside root segments (as in finite-difference approach) is released.

Table 1
Summary of the assumptions made by each of the resolution method, the preparatory steps and the equations to be solved when applying a potential or a flux boundary condition at the root system collar.

	Uniform $\Psi_{sr,i}$	Uniform $\Psi_{x,i}$	Simplified compensatory RWU	Preparatory calculation	Flow resolution (Potential collar BC)	Flow resolution (Flux collar BC)
Finite-difference	x	x		Build **C** and **D** or Build **c** and **d**	Eqs. (3.1)–(3.3)	Eqs. (3.2)–(3.3)
Macroscopic	x	x	x	Build **C** and **D** (or **c** and **d**) and Calc. K_{rs}, **SUF** and K_{comp}	Eqs. (3.4)–(3.5)	Eq. (3.4)
Hybrid	x			Build **A** and **b** or Build **a** and **b**	Eq. (3.12)	Eq. (3.13)
Hybrid macroscopic	x		x	Build **A** and **B**(or **a** and **b**) and Calc. K_{rs}, **SUF** and K_{comp}	Eqs. (3.4)–(3.5)	Eq. (3.4)

2.2.1. Hybrid water flow solution

As it can be directly seen from Eqs. (10) and (11), the solution of the water flow equation is linear in terms of distal flow and proximal water potential so that for root system architecture, we can gather a set of **N+1 linear equations** that can be numerically solved:

$$\begin{bmatrix} \Psi_{collar} \\ \boldsymbol{\Psi}_{\mathbf{x}0} \end{bmatrix} = \mathbf{A}^{-1}.\mathbf{B} \tag{12}$$

where **A** [N+1 × N+1] and **B** [N+1 × 1] are constructed using Eqs. (10) and (11) and the incidence matrix **IM**, $\boldsymbol{\Psi}_{\mathbf{x}0}$ [N × 1] is the vector of $\Psi_{x0,i}$. Appendix D explains in details how to build this matrix.

When imposing a potential boundary condition at the root system collar instead of a flux one, the water flow equation solution in the root system becomes:

$$\boldsymbol{\Psi}_{\mathbf{x}0} = \mathbf{a}^{-1}.\mathbf{b} \tag{13}$$

where **a** [N × N] and **b** [N × 1] are fully described in Appendix D. **a** is **A** without its first line and row.

Fig. 1c illustrates the same root system as the one presented in Fig. 1a. With the hybrid water flow solution formulation, the root system must be split either when root hydraulic property change (due for example to root tissue maturation) or at root branching sites. The total number of zones is here reduced to 11. Each single zone (as the one highlighted in the frame of Fig. 1d) is characterized by its intrinsic hydraulic properties: radial conductivity ($k_{r,i}$) and axial intrinsic conductance ($k_{x,i}$) and its geometrical characteristics: zone length and zone radius. We then need to determine 2 unknowns per root zone: the distal potential and the proximal flow (in blue in Fig. 1). A set of linear Eqs. ((12) or (13)) can be solved depending on the boundary conditions (in red in Fig. 1).

2.2.2. Hybrid macroscopic parameters calculation

As it was done in Section 2.1.2., the exact water flow solution can be used to calculate the macroscopic parameters of the Couvreur model. Solving Eqs. (12) or (13) under homogeneous soil conditions leads to K_{rs} and **SUF** while K_{comp} can be calculated when the water flows in the root system are known under heterogeneous soil conditions. We show in Appendix E that K_{rs} and **SUF** can be calculated analytically as well. So K_{comp} remains the only non-exact macroscopic parameter of this approach.

2.3. Summary of all solutions and assumptions

Table 1 summarizes the four approaches detailed in Sections 2.1.1. (Finite-difference approach), 2.1.2 (Macroscopic), 2.2.1 (Hybrid) and 2.2.2 (Hybrid macroscopic) and associated assumptions. It also describes the preparatory work required before generating a solution of the water flow equations in a RSHA. We call preparatory work all the tasks that need be done when either the root system architecture (e.g. growth, senescence) or the hydraulic properties (e.g. maturation, circadian cycle) change. The flow resolution includes the steps to calculate the water flow and xylem potential everywhere in the RS when the preparatory work has been already processed. The flow resolution steps need to be repeated whenever the boundary conditions change. Finally, in Table 1, the equations to solve the water flow equations in RSHA under either flux or potential top boundary conditions are provided as well.

Table 1 also includes the assumptions made by each resolution method. All models first assume that the potential at the soil-root interface is uniform for each single segment, i.e., the soil-root potential can differ between segments but must remain homogeneous for a particular root segment. The macroscopic approaches then include a non-exact parameter for describing the compensatory RWU. Finally the finite-difference (and therefore the macroscopic) method impose a constant potential within each single segment while this assumption is released in the hybrid model (and therefore the hybrid macroscopic).

3. Material and methods

In this section we describe the tests designed to assess the impact of using the finite-difference approach as compared to a hybrid method:

(i) on the local water flow, the plant transpiration and the root macroscopic parameters in static conditions (Section 3.1.);
(ii) on dynamic variables of the root-soil continuum that are generated using a coupled model of the water flow in the root system and in the soil (Section 3.2.).

On total, five tests are presented illustrating the range of numerical errors that we deal with when using the Doussan model. All root systems used in this study are generated using RootTyp [38] and maize root system parameters [50]. For the dynamic tests, we used R-SWMS as coupled soil-root system model [17].

3.1. Discretization error and computational time in static conditions

Test 1: Impact of the radial to axial conductivity ratio

For the first test, we compute water flow in an 80-days old maize root system architecture for a prescribed water potential at plant collar ("potential boundary condition"). Segmentation lengths from 0.01 cm to 1 cm are tested. Results are compared in terms of (i) relative computational time and (ii) numerical accuracy of the calculated flow rate at plant collar resulting from the applied boundary condition. The former is the ratio of CPU times between the finite-difference and hybrid solutions (including the matrix building and parameter calculation steps). The numerical accuracy is the relative difference in percent between flow rates at plant collar calculated from both approaches, which is equivalent to the relative error on the total root system conductance.

In order to analyze the impact of the root radial to axial conductivity ratio $\frac{k_r}{k_x}$ (from 0.0001 cm^{-3} to 1 cm^{-3}), we used homogeneous hydraulic properties, i.e., constant with root age and order. More realistic hydraulic properties profiles are used in the next tests, whose root systems do not have unique $\frac{k_r}{k_x}$ ratios.

Test 2: CPU time and error variability in growing maize root systems

The second test assesses the variability of the model error resulting from the constant potential assumption in root systems with non-uniform hydraulic properties, and separates the components of the computational time of each approach. We used the software RootTyp [38] to generate 100 maize phenotypes contrasted in terms of architectural and hydraulic properties. These properties were randomly selected from a parametric space delimiting the natural variability range of maize hydraulic and architectural properties reported in the literature (for more information, see [50]). We solved water flow equations at daily stages of root system development over 60 days with average segment lengths of 0.5 cm. For each approach, we distinguished the mean time to prepare the calculations (building the conductance matrices, see Appendices A and D) and to solve the water flow problem (see Section 2.3.). The model error was quantified as the difference between root system conductances (K_{rs}) obtained from hybrid and finite-difference approaches. We were then able to compare the variability of the model error to the "natural variability" of K_{rs} within the species.

Test 3: Assessing errors applied to experimental data

In a third test, we assess how root system segmentation might affect interpretations of experimental observations of water uptake patterns. In practice, Zarebanadkouki et al. [15] measured distributed root water uptake rates and total transpiration, then searched for root hydraulic properties profiles that best reproduce the experimental observations through root water uptake dynamics simulations (i.e., "inverse modeling"). Here we use a lupine root system architecture experimentally digitalized [15] and three different segmentation lengths for the Doussan model: 0.025, 0.25 and 2.5 cm. The homogeneous soil-root interface potential of −100 cm measured experimentally [15] was applied as boundary condition for root segments. At the plant collar, a potential of −2500 hPa was measured by pressure probe and set as top boundary condition. Eventually, we quantify, for the same optimal root hydraulic properties [15], how the simulated uptake pattern deviates from the original as a result of the finite difference model segmentation.

3.2. Propagation of discretization errors in coupled soil-plant models

Test 4: Root discretization impact on simulated water supply to the shoot

Using the same RS architecture as in the first test, we first ran simulations starring an 80 days-old maize root system whose total root length was 600 m. We used two segment lengths to discretize the root system: 0.1 cm and 1 cm. The root system was placed in a loamy soil at field capacity with no other water supply than soil water storage. The potential daily transpiration was fixed to 5.33 mm of water (with sinusoidal changes through day-night cycles, see [26]). We also defined a minimal collar potential (−15,000 hPa) beyond which transpiration cannot meet the atmospheric demand. At the onset of water stress, the top boundary condition was switched from prescribed flux to constant water potential. Soil water flow was calculated with Richards equation [51]. Its coupling with root water dynamics is described in further details in [17,26].

In a second series of simulations, we quantified the impact of maize root discretization on soil-root system water supply to the shoot over a two-month period. We used measured weather data from a French weather station located

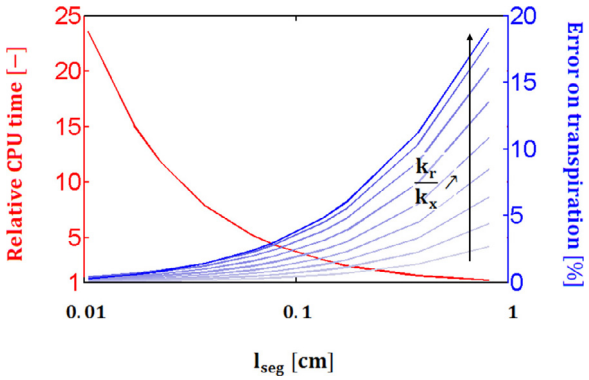

Fig. 2. Finite-difference model relative error on plant transpiration calculation (blue curves) and relative CPU time (red curve) as a function of segmentation length. The figure presents results for different ratios of radial to axial conductivities (the darker, the higher the ratio). (For interpretation of the references to colour in this figure legend, the reader is referred to the web version of this article.)

near Montpellier to calculate the daily potential transpiration. No feedback between plant water status and growth was accounted for (i.e., the actual growth rate is equivalent to the potential one). For further details on the scenario, see [50].

Test 5: Impact of root segmentation on state variables of the soil-plant system

In the last test, we used the two root system phenotypes, generated in the second test, that were the most contrasted in terms of numerical error (minimal and maximal) to simulate the water flow in the soil-root-atmosphere continuum**,** hereafter referred to as phenotype min and max, respectively. We considered three root system ages: 20, 40 and 60 days and simulated water flow using the Couvreur et al. model with macroscopic parameters calculated either with the hybrid model or with the finite-differences approach in an initially homogeneous loamy soil. We used a sinusoidal transpiration function (maximal transpiration at midday, zero transpiration at midnight) with potential daily transpiration of 0.35 mm, 2.67 mm and 5.33 mm, respectively for the three ages. The minimal collar potential was anew fixed to −15,000 hPa for all root systems and ages. Two initial soil conditions were considered: −300 hPa and −3000 hPa with an initial hydrodynamic equilibrium. We focused our analysis on key variables calculated by the root-soil model: the mean soil water content in the soil, the RS sink term, the cumulative transpiration and the collar potential. The relative differences between outputs of the two models were normalized by state variable calculated with the hybrid solution (respectively the mean soil water content, the mean sink term, the final cumulative transpiration, and the plant collar potential at the onset of water stress).

4. Results

In this section, we highlight the benefits of using the hybrid solution presented above. With examples we show when and how significant errors may emerge from the finite-difference approach with low spatial resolution.

Test 1: Impact of the radial to axial conductivity ratio

The flow rate at plant collar calculated with the finite-difference approach with the mature maize root system was off by up to 20% relative to the hybrid exact solution (see blue curves in Fig. 2). Yet, the relative error asymptotically tended to zero with finer root segmentation (and larger segment number), the hybrid solution being equivalent to that of an infinitesimal root segmentation. However, using fine root segmentations with the finite-difference method required higher computational times (24-fold for the 0.01 cm segmentation, see red curve in Fig. 2). The hybrid solution was faster than the finite-difference approach regardless of discretization, though computing times were fairly similar above 0.5 cm segmentation.

The position of lighter versus darker blue curves highlights that segmentation errors dramatically change with root hydraulic properties. For any given segmentation, the relative error varied by one order of magnitude from lowest to highest ratios of radial to axial conductivity (see blue curves in Fig. 2). Highest ratios yielded the largest errors. The assumption of constant water potential inside a root segment (inherent to the Doussan model) is indeed farther from being satisfied if axial pressure head losses are relatively important (low axial conductivity or high radial conductivity), particularly in longer root segments. As segmentation lengths of 1 cm are common in current models, typical simulations of root water uptake are likely subject to substantial errors. Mathematical criteria for optimal root segment length were discussed by Meunier et al. [52], who indicate that the product of the segment length by its inherent hydraulic property τ should not be larger than 1 to avoid large errors.

Test 2: CPU time and error variability in growing maize root systems

Preparatory calculation times (i.e., building the conductance matrices) were two to four orders of magnitude larger than the time necessary to solve the flow solution (see Fig. 3, panel A versus B). This first step is required when the root system hydraulic architecture changes (e.g. root growth, development or senescence) but not when the boundary conditions alone evolve. Hence, there is a noteworthy tradeoff between the update of root system properties and the CPU time, particularly

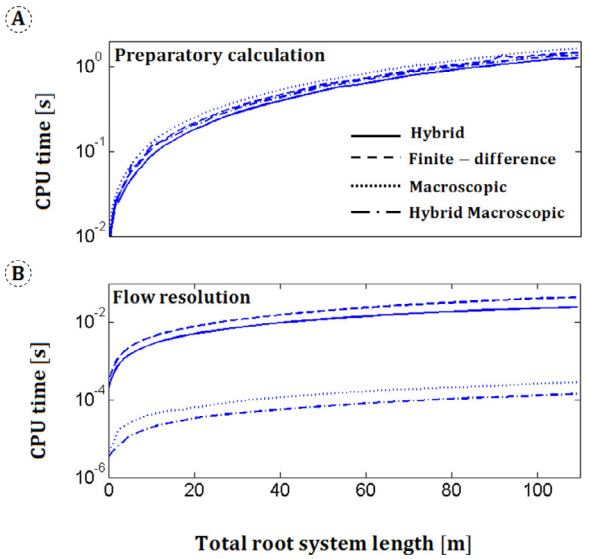

Fig. 3. Comparison of the different methods in terms of computational time in growing root systems. The CPU time for preparatory calculations is shown in subplot A, while the flow solution CPU time is represented in subplot B.

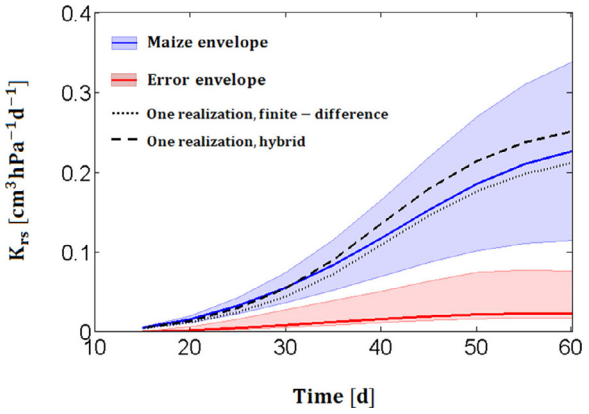

Fig. 4. Simulated natural variability of maize root system conductance (blue solid line: average; blue envelope: standard deviation) in a population of 100 phenotypes growing for 60 days. The associated finite difference model (using 0.5 cm segments) mean absolute error is shown in red (the envelope encompasses the 5% to 95% percentiles of errors). An example of phenotype root system conductances calculated with the hybrid (dashed black line) and finite-difference (dotted black line) approaches is included. (For interpretation of the references to colour in this figure legend, the reader is referred to the web version of this article.)

with the macroscopic models (see dotted and dashed-dotted curves in Fig. 3 B) whose second step is two orders of magnitude faster because they do not involve a matrix inversion [26]. However, if preparatory calculations are needed, the fastest and most accurate method is always the hybrid approach (see solid lines in Fig. 3).

Fig. 4 displays in blue the evolution of root system conductance (K_{rs}) over time in the 100 maize phenotypes covering the natural variability of hydraulic and architectural traits. The blue envelope encompasses ± one standard deviation of the population K_{rs}. The mean absolute finite difference model error (red solid line in Fig. 4, discretization of 0.5 cm) was 10% of K_{rs} on average, with 90% of errors comprised between 8 and 40% of K_{rs} (red envelope) after 60 days. This error is relatively high as compared to the estimated intraspecies variability (±50% of K_{rs}, blue envelope).

As shown in Fig. 2, the relative model error depends on the local hydraulic properties of the root system which are phenotype key-traits. Consequently comparing contrasted phenotypes is automatically biased when using the finite difference method. This is also illustrated in Fig. 4 where the black curves represent the evolutions of K_{rs} of a representative phenotype using the hybrid (dashed) and finite difference (dotted) methods. Such differences do affect the results of virtual phenotype performance prospects under drought scenarios, as proposed in [50].

Test 3: Assessing errors applied to experimental data

In Fig. 5, we mapped deviations of root water uptake as compared to the hybrid solution from coarse (2.5 cm) to fine (0.025 cm) segmentations. The root segment colors represent the relative error on the radial flux: blue means that the

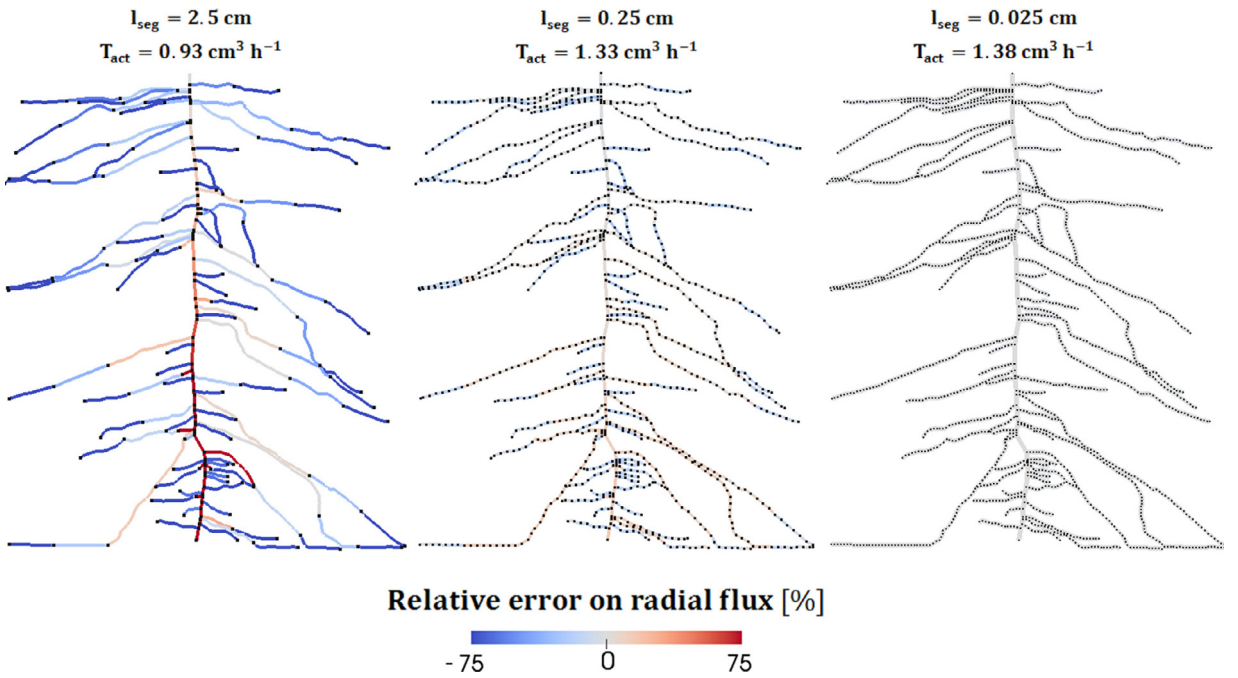

Fig. 5. Segment size effect on local and total water uptake for three discretization levels (from coarse to fine, from left to right). The segment limits are indicated by black dots on the root laterals only.

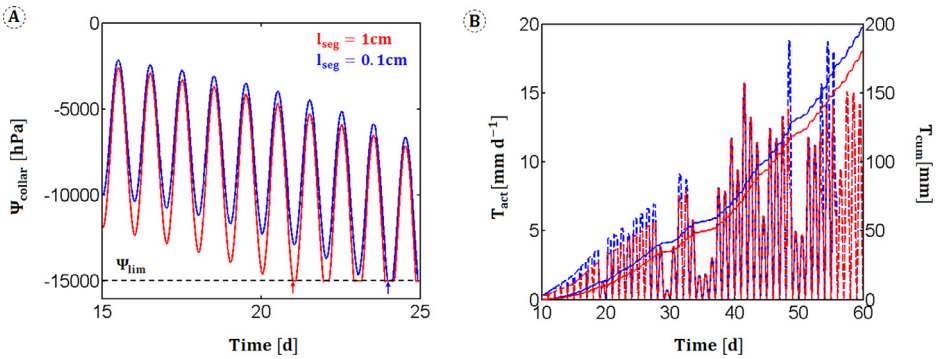

Fig. 6. Simulated soil-plant water dynamics time series for 1 cm (red) and 0.1 cm (blue) segmentations. Panel A: Plant collar water potential. Red and blue arrows point at specific times of onset of water limitation. Panel B: Instantaneous (left axis) and cumulative (right axis) water supply from the soil-root system to the shoot. (For interpretation of the references to colour in this figure legend, the reader is referred to the web version of this article.)

Doussan model underestimates the water uptake and red means that it overestimates it. When the Doussan and the hybrid models agree, segments appear gray. We also indicated the numerical error made on the plant total transpiration that reaches 33% of the global transpiration with coarse segments, 3.6% with intermediate segments and less than 0.1% with very fine segments. With segmentation lengths of the order of the centimeter, numerical errors would cause dramatic bias in the estimated root hydraulic properties, while the true hydraulic properties would be far from matching the observed uptake and transpiration rates as shown in the left panel.

While numerical errors tend to disappear in the right panel, the computation time explodes, which is a major issue in any inverse modeling scheme as tens of thousands simulations are typically necessary before reaching the optimal parameter set. The hybrid method does not have such a limitation as it yields the exact solution with coarse segments.

Test 4: Root discretization impact on simulated water supply to the shoot

In this test, the simulations of the water flow in the soil-root continuum are rigorously identical except for the root segment length. As shown in Fig. 6A, the discretization size (red = 1 cm, blue = 0.1 cm) led to significant differences in the onset of water limitation. In case of finer segments, the stress appeared 3 days later (see red versus blue arrows). This is due to the discretization effect on root system conductance, which is underestimated by 20% with the coarse segmentation, thus limiting water supply to the shoot.

Table 2
Main relative differences between soil-plant model state variables. The simulations ran with macroscopic parameters calculated using the Doussan model or the hybrid model for two phenotypes generating maximum and minimum model errors at three different ages and under wet or dry condition. All numbers are in %.

			Young RS				Intermediate RS				Old RS			
			Phenotype max		Phenotype min		Phenotype max		Phenotype min		Phenotype max		Phenotype min	
			Dry	Wet	Dry	Wet	Dry	Wet	Dry	Wet	Dry	Wet	Dry	Wet
Relative Error on	Water content	Min	0.51	1.95	0.18	0.12	0.29	0.33	0.07	0.03	0.2	0.26	0.04	0.01
		Max	2.1	4.11	0.25	0.45	1.23	3.82	0.21	0.38	1.26	3.06	0.15	0.27
	Sink term	Min	13.46	24.94	1.87	1.57	22.44	25.52	2.48	2.36	21.15	25.97	1.86	1.86
		Max	25.03	40.95	3.43	2.41	53.76	27.34	9.37	5.37	36.29	29.07	9.67	2.23
	Total transpiration	Min	0	−0.02	0	0	−0.01	−0.01	−0.01	0	−0.01	0	0	0
		Max	1.64	0	0.38	0.01	2.26	0.01	0.75	0.01	2.05	0.02	0.35	0
	Collar potential	Min	−9.71	−16.59	−1.3	−1.61	−10.54	−13.36	−1.57	−1.61	−9.86	−10.33	−0.94	−0.6
		Max	1.46	4.81	0.31	0.33	1.36	0	0.1	−0.01	2	0.28	0.04	0

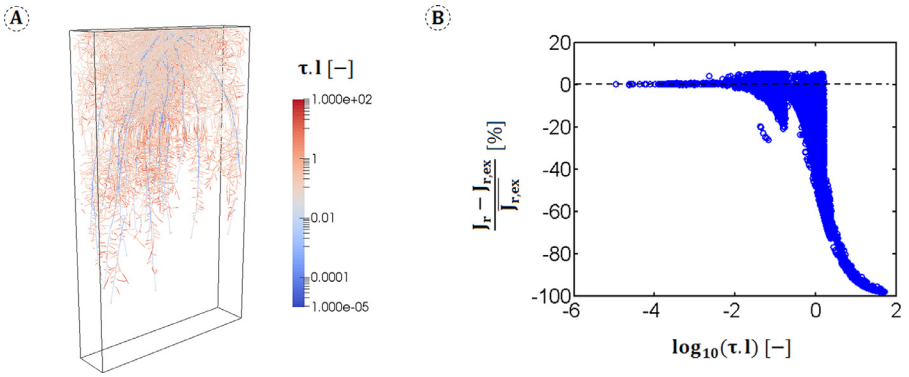

Fig. 7. Distribution of the segment property τl as proxy of the water uptake error pattern in a virtual maize root hydraulic architecture (panel A). Relation between relative model error on the local water uptake rate and the segment property τl (panel B).

In the two-month scenario with growing root system, segmentation differences led to the actual (left axis, dashed blue lines) and cumulative (right axis, solid red lines) transpiration represented at Fig. 6B. The difference of cumulative water supply after two months is about 15 mm of water. It was mainly constituted early stages of root system growth, when the xylem vessels are not developed yet (and the radial to axial conductivity ratio is high, hence generating large model errors, see Test 1).

Test 5: Impact of root segmentation on state variables of the soil-plant system

Finally, Table 2 summarizes minimal and maximal differences for several normalized state variables of a soil-plant hydraulic model [17] run with macroscopic parameters calculated with the hybrid and finite difference models. As it clearly appears, after normalization, errors are far from being negligible since they may represent up to 4% of the mean water content, 41% percent of the mean sink term, 2% of the total transpired water and 16% of the stress potential. As explained before, the hydraulic properties of the root systems dramatically affect the accuracy of the water flow resolution and hence the description of the water fluxes in the soil-plant-atmosphere continuum. There, even if not negligible most of the time, the errors on state variables of the phenotype min are always smaller (i.e., closer to zero) than those of the phenotype max.

In Fig. 7A, the intrinsic property of the root segment τ_i multiplied by the segment length l_i is shown for the old root system of the phenotype max. Fig. 7B represents the relative errors of root water uptake in the same 60 days-old maize root system presented as a function of this product $\tau_i l_i$. The errors are calculated as the relative difference of root radial flow $\mathbf{J_r} - \mathbf{J_{r,ex}}$, (with the second term calculated with the hybrid solution and the first with the finite-difference approach, weighted by the mean exact radial flow $\mathbf{J_{r,ex}}$). As discussed in [52], $\tau_i l_i$ is an indicator of the potential error of local water uptake, the error being located where the product $\tau_i l_i$ is high. When the root segment size is uniform within the root system (as it is here), the main errors are located at the lateral root tips, where the radial to axial conductivity ratio is the highest (and therefore τ_i is large). Let us note finally that the use of the finite-difference approach will always underestimate the root system total inflows under top potential boundary condition.

5. Conclusion

We developed and presented a hybrid solution of the water flow inside root system of any complexity under flux or potential boundary conditions. This method is based on the extension of the Landsberg and Fowkes [9] resolution of the water flow equation in a single root segment combined with a finite-difference approach of Doussan et al. [14]. The hybrid approach improves the solution accuracy of transpiration fluxes as compared to traditional finite-difference model up to 35%, with improved computational speed. In order to contain the finite-difference model error below 5%, the root system segmentation would have to be finer than 0.1 cm, which would imply 10 to 100-fold increases in CPU time as compared to the hybrid solution. The new methodology is the asymptotic solution of traditional resolution methods for infinitely small segments (and for infinite segment number), and can be implemented in any functional-structural root system model (as for instance SimRoot [53]). The finite-difference method generates substantial errors on shoot water supply and water uptake location and intensity, which may result in erroneous estimations of root hydraulic properties from experimental observations of plant water uptake. A new solution of plant scale parameters K_{rs} and SUF has also been provided, which opens the possibility to swiftly characterize virtual phenotypes hydraulic traits, and more accurately prospect on root ideotypes for water extraction in drought scenario analysis.

Acknowledgments

F.M. is supported by "Fonds National de la Recherche Scientifique" of Belgium (FNRS) as Research Fellow and is grateful to this fund for its support. During the preparation of this manuscript, V.C. was supported by the "Belgian American Educational Foundation" (BAEF) as UCLouvain Fellow, by "Wallonie-Bruxelles International" (WBI) with a WBI.WORLD excellence grant, and by the "Fonds Spéciaux de Recherche" (FSR) of the Université catholique de Louvain with a post-doctoral grant complement. This work was also supported by the Belgian French community ARC 16/21–075 project.

Appendix A. Description of the IM, C, D, c and d matrices

We first introduce the incidence matrix as it was done in the work of Doussan et al. [14]. This matrix, **IM** [N+1 × 2 N] (-), contains the information on connections between root segments and soil-root interfaces of the hydraulic architecture. In order to build the **C** matrix, only the upper half of the incidence matrix described by Doussan et al. [14] is necessary.

$$\mathbf{IM} = \begin{bmatrix} \mathbf{-1} & 0 & \cdots & \cdots & \cdots & 0 & 0 & 0 & \cdots & \cdots & \cdots & 0 \\ 1 & \mathbf{-1} & & & & \vdots & 1 & 0 & \cdots & \cdots & \cdots & 0 \\ 0 & 1 & & & & 0 & 0 & 1 & \ddots & & & \vdots \\ \vdots & \ddots & \ddots & & & \mathbf{-1} & \vdots & \ddots & \ddots & \ddots & & \vdots \\ \vdots & & \ddots & \ddots & & 0 & \vdots & & \ddots & \ddots & \ddots & \vdots \\ \vdots & & & \ddots & \ddots & \vdots & \vdots & & & \ddots & \ddots & 0 \\ 0 & \cdots & \cdots & \cdots & 0 & 1 & 0 & \cdots & \cdots & \cdots & 0 & 1 \end{bmatrix} \tag{A.1}$$

Each line of **IM** corresponds to a root segment. The first line is that of the collar, while the N next lines correspond to the ordered N segments. The N first columns of **IM** correspond to the ordered N segments, while the next N columns correspond to the ordered N soil-root interfaces. **IM** is almost full of zeros, with ones on the main diagonals of both square sub-matrices located below the first line (see Eq. (A1)), which represent connections of segments with themselves and with soil-root interfaces. The first *N* columns contain each an additional "−1", which represent the connection of each segment with the previous segment in the architecture. $IM_{i+1,j}$ is "−1" if the *i*-th segment is the parent of the *j*-th segment in the architecture (each segment having only one parent). For instance, in the first column, the collar appears to be the parent of the first segment. In the second column, the first segment appears to be the parent of the second segment. Note that the third segment could have either the first or the second segment as parent. Since segments are ordered, the lower half of the first square sub-matrix can only contain zeros (the third segment could, for instance, not be the parent of the first segment).

We then define the conductance matrix **C** [N + 1 × N + 1] (L^3 P^{-1} T^{-1}) by:

$$\mathbf{C} = \mathbf{IM}.\mathbf{diag}\left(\begin{bmatrix} -\mathbf{K_x} \\ -\mathbf{K_r} \end{bmatrix}\right).\mathbf{IM^t}$$

where $\mathbf{diag}([\begin{smallmatrix} -\mathbf{K_x} \\ -\mathbf{K_r} \end{smallmatrix}])$ [2 N × 2N] is a diagonal matrix containing the root segment axial and radial conductances on its diagonal and is 0 elsewhere . The vector **D** [N+1 × 1] (L^3 T^{-1}) is defined as:

$$\mathbf{D} = \begin{bmatrix} T_{act} \\ \mathbf{diag}(-\mathbf{K_r}).\ \mathbf{\Psi_{sr}} \end{bmatrix}$$

where T_{act} (L^3T^{-1}) is the boundary condition for the root collar (flux condition), $\mathbf{diag}(-\mathbf{K_r})$ [N × N] ($L^3\ P^{-1}\ T^{-1}$) is a square matrix which contains $\mathbf{K_r}$ on its diagonal and is zero elsewhere and $\mathbf{\Psi_{sr}}$ [N × 1] (P) contains the boundary conditions for the root segments.

In case of a top potential boundary condition, the root water flow equations are slightly modified. $\mathbf{c}$ [N × N] is $\mathbf{C}$ without its first line and column and $\mathbf{d}$ [N × 1] ($L^3\ T^{-1}$) is defined as:

$$\mathbf{d} = \left(\mathbf{diag}(-\mathbf{K_r}).\ \mathbf{\Psi_{sr}} - \begin{bmatrix} K_{x,1}.\ \Psi_{collar} \\ 0 \\ \vdots \\ 0 \end{bmatrix} \right)$$

with Ψ_{collar} (P) the potential boundary condition for the root collar.

Appendix B. Exact solution in a root zone

The solution of the water flow equation in a root branch as derived by Landsberg and Fowkes [9] for generic boundary conditions is:

$$\Psi_{x,i}(z) = \Psi_{sr,i} + c_{1,i}\cosh(\tau_i z) + c_{2,i}\sinh(\tau_i z) \tag{B.1}$$

The axial water flow is powered by the potential gradient inside the xylem vessels and is given by:

$$J_{x,i}(z) = -k_{x,i}\frac{d\Psi_{x,i}(z)}{dz} = -\kappa_i\ (c_{1,i}\sinh(\tau_i z) + c_{2,i}\cosh(\tau_i z)) \tag{B.2}$$

where κ_i ($L^3P^{-1}T^{-1}$) is defined as:

$$\kappa_i = \sqrt{2\pi r_i k_{r,i} k_{x,i}} \tag{B.3}$$

We apply a potential $\Psi_{proximal,i}$ (P) and a flux $J_{distal,i}$ (L^3T^{-1}) conditions respectively at the top (proximal end) and bottom (distalend) borders of this root cylinder, mathematically:

$$\begin{cases} \Psi_{x,i}(z = l_i) = \Psi_{proximal,i} \\ J_{x,i}(z = 0) = J_{distal,i} \end{cases} \tag{B.4}$$

Eqs. (B1) and (B2) yield:

$$\begin{cases} \Psi_{proximal,i} = \Psi_{sr,i} + c_{1,i}\cosh(\tau_i l_i) + c_{2,i}\sinh(\tau_i l_i) \\ J_{distal,i} = -\kappa_i\ c_{2,i} \end{cases} \tag{B.5}$$

Solving Eq. (B5) for both coefficients writes:

$$\begin{cases} c_{1,i} = \dfrac{\Psi_{proximal,i} - \Psi_{sr,i} + \frac{J_{distal,i}}{\kappa_i}\sinh(\tau_i l_i)}{\cosh(\tau_i l_i)} \\ c_{2,i} = -\dfrac{J_{distal,i}}{\kappa_i} \end{cases} \tag{B.6}$$

The coefficients can be inserted in Eqs. (B1) and (B2) to obtain the distal potential $\Psi_{x0,i}$ and the proximal flow $J_{xl,i}$ of the root branch:

$$\Psi_{x0,i} = \Psi_{x,i}(z = 0) = \Psi_{sr,i} + \frac{\Psi_{proximal,i} - \Psi_{sr,i} + \frac{J_{distal,i}}{\kappa_i}\sinh(\tau_i l_i)}{\cosh(\tau_i l_i)} \tag{B.7}$$

$$J_{xl,i} = J_{x,i}(z = l_i) = \left(-\Psi_{proximal,i} + \Psi_{sr,i} - \frac{J_{distal,i}}{\kappa_i}\sinh(\tau_i l_i)\right)\kappa_i\tanh(\tau_i l_i) + J_{distal,i}\cosh(\tau_i l_i) \tag{B.8}$$

Appendix C. Exact solution in a root zone for top-flux boundary condition

We apply a flux $J_{proximal,i}$ (L^3T^{-1}) at the top (proximal end) of a root branch as well as a flux $J_{distal,i}$ (L^3T^{-1}) at its bottom (distal end), mathematically:

$$\begin{cases} J_{x,i}(z = l_i) = J_{proximal,i} \\ J_{x,i}(z = 0) = J_{distal,i} \end{cases} \tag{C.1}$$

Combining the boundary conditions C1 with Eq. (B2), it yields:

$$\begin{cases} J_{proximal,i} = -\kappa_i\ (c_{1,i}\sinh(\tau_i l_i) + c_{2,i}\cosh(\tau_i l_i)) \\ J_{distal,i} = -\kappa_i\ c_{2,i} \end{cases} \tag{C.2}$$

Solving C2 writes

$$\begin{cases} c_{1,i} = \dfrac{-J_{proximal,i} + J_{distal,i}\cosh(\tau_i l_i)}{\kappa_i\ \sinh(\tau_i l_i)} \\ c_{2,i} = -\dfrac{J_{distal,i}}{\kappa_i} \end{cases} \tag{C.3}$$

Appendix D. Description of the A, B, a and b matrices

Top flux boundary condition

To construct matrix **A** $[N+1 \times N+1]$, we use the subscripts j that vary between 1 and N. **A** is a sparse matrix which is zero everywhere, except at the following locations:

$$A(i+1,i+1) = A(i+1,i+1) - \frac{\kappa_j}{\sinh(\tau_j l_j)} - \kappa_j \tanh\left(\frac{\tau_j l_j}{2}\right) \quad \text{if j is connected to i}$$

$$A(j+1,i+1) = A(j+1,i+1) + \frac{\kappa_j}{\sinh(\tau_j l_j)} \quad \text{if j is connected to i}$$

$$A(i+1,j+1) = A(i+1,j+1) - \kappa_j \tanh\left(\frac{\tau_j l_j}{2}\right) + \frac{\kappa_j}{\tanh(\tau_j l_j)} \quad \text{if j is connected to i}$$

$$A(j+1,j+1) = A(j+1,j+1) - \frac{\kappa_j}{\tanh(\tau_j l_j)} \quad \text{if j is connected to i}$$

For **B** $[N+1 \times 1]$, we must distinguish segments connected to the root system collar from those that are not.

$$B(i+1,1) = B(i+1,1) - \Psi_{sr,j}\, \kappa_i \tanh\left(\frac{\tau_j l_j}{2}\right) \quad \text{if j is connected to i}$$

$$B(j+1,1) = B(j+1,1) - \Psi_{sr,j}\, \kappa_i \tanh\left(\frac{\tau_j l_j}{2}\right) \quad \text{if j is connected to i}$$

$$B(i,1) = B(i,1) + J_{collar} \quad \text{if i is connected to the collar}$$

Top potential boundary condition

a $[N \times N]$ is **A** without its first line and column.

For **b** $[N \times 1]$, we must distinguish segments connected to the root system collar (i in the following lines) from those that are not (j). Again i and j indices can vary between 1 and N.

$$b(i,1) = b(i,1) - \Psi_{sr,i}\, \kappa_i \tanh\left(\frac{\tau_i l_i}{2}\right) \quad \text{if j is connected to i}$$

$$b(j,1) = b(j,1) - \Psi_{sr,j}\, \kappa_i \tanh\left(\frac{\tau_j l_j}{2}\right) \quad \text{if j is connected to i}$$

$$b(i,1) = b(i,1) - \Psi_{collar} \frac{\kappa_i}{\sinh(\tau_i l_i)} \quad \text{if i is connected to the collar}$$

Appendix E. Exact calculation of parameters K_{rs} and SUF

The exact solution of the water flow equation can also be used to calculate the macroscopic parameters of the Couvreur model instead of using the Doussan equations. We calculate the root system flow and xylem water potential under homogeneous soil-root interfaces conditions: $\boldsymbol{\Psi_{sr}} = \Psi_{seq}$, with Ψ_{seq} (P) a constant. Under this condition, the distal flow can be related to the upstream conductance $K_{rs,i+1}$ by:

$$J_{distal,i} = K_{rs,i+1}(\Psi_{sr,i} - \Psi_{x0,i}) \tag{E.1}$$

The axial flow at the top of this segment is given by equation B2 evaluated in $z = l_i$. It yields

$$J_{xl,i} = -\kappa_i(c_{1,i}\sinh(\tau_i l_i) + c_{2,i}\cosh(\tau_i l_i)) \tag{E.2}$$

The difference of potential between the soil-root interface and the proximal end of this segment is calculated using Eq. (B1). It writes:

$$\Psi_{seq} - \Psi_{xl,i} = -(c_{1,i}\cosh(\tau_i l_i) + c_{2,i}\sinh(\tau_i l_i)) \tag{E.3}$$

The conductance of the root system including the upstream conductance and the present segment i, $K_{rs,i}$ ($L^3T^{-1}P^{-1}$) is given, in homogeneous conditions, by the total axial flow divided by the potential difference between the soil-root interface and the proximal end. Dividing Eq. (E2) by Eq. E3, we obtain:

$$K_{rs,i} = \frac{J_{xl,i}}{(\Psi_{xl,i} - \Psi_{seq})} = \kappa_i \frac{(c_{1,i}\sinh(\tau_i l_i) + c_{2,i}\cosh(\tau_i l_i))}{(c_{1,i}\cosh(\tau_i l_i) + c_{2,i}\sinh(\tau_i l_i))} \tag{E.4}$$

Combining Eq. (B1) evaluated in $z = 0$ and Eq. (E1), the distal flow yields:

$$J_{distal,i} = -K_{rs,i+1}\, c_{1,i} \tag{E.5}$$

Eq. (B5) allows one calculating the second coefficient $c_{2,i}$:

$$c_{2,i} = \frac{K_{rs,i+1}}{\kappa_i} c_{1,i} \tag{E.6}$$

Combining Eqs. (E4) and (E6), it yields:

$$K_{rs,i} = \kappa_i \left(\frac{\kappa_i \sinh(\tau_i l_i) + K_{rs,i+1} \cosh(\tau_i l_i)}{\kappa_i \cosh(\tau_i l_i) + K_{rs,i+1} \sinh(\tau_i l_i)} \right) \tag{E.7}$$

When no initial conductance is attached to the distal end of the system, Eq. (E7) simply becomes:

$$K_{rs,i} = \kappa_i \tanh(\tau_i l_i) \tag{E.8}$$

which is the formula derived by Landsberg and Fowkes in 1978 [9].

It appears that the root system conductance can be calculated recursively from the root tip towards the root collar. The first conductance $K_{rs,1}$ is the total root system conductance K_{rs}. When calculated for all cumulative root zones from the root tips to the root collar, the root conductances can then be used to obtain the xylem potential, starting from the root collar to the root tips combining Eqs. (B1), (B6) and (E5):

$$\Psi_{x,i}(z) = \Psi_{seq} + \left(\Psi_{proximal,i} - \Psi_{seq}\right) \frac{\kappa_i \cosh(\tau_i z) + K_{rs,i+1} \sinh(\tau_i z)}{\kappa_i \cosh(\tau_i l_i) + K_{rs,i+1} \sinh(\tau_i l_i)} \tag{E.9}$$

$\Psi_{proximal,i}$ is derived from the previous calculations: it is calculated evaluating Eq. B1 in $z = 0$. Eq. (E9) is used to calculate the next proximal potential by taking anew $z = 0$:

$$\Psi_{proximal,i+1} = \Psi_{seq} + \left(\Psi_{proximal,i} - \Psi_{seq}\right) \frac{\kappa_i}{\kappa_i \cosh(\tau_i l_i) + K_{rs,i+1} \sinh(\tau_i l_i)} \tag{E.10}$$

Finally the radial flow is given by the integral of the radial flux per unit of length:

$$J_{r,i} = \int_0^{l_i} -2\pi r_i k_{r,i} (\Psi_{seq} - \Psi_{x,i}(z)) \, dz \tag{E.11}$$

Combining Eqs. (E9) and (E11), we obtain:

$$J_{r,i} = \kappa_i \left(\Psi_{proximal,i} - \Psi_{seq}\right) \frac{(\kappa_i \sinh(\tau_i l_i) + K_{rs,i+1} \cosh(\tau_i l_i) - K_{rs,i+1})}{\kappa_i \cosh(\tau_i l_i) + K_{rs,i+1} \sinh(\tau_i l_i)} \tag{E.12}$$

The radial flows as calculated by Eq. (E.12) can be used to calculate the Standard Uptake Fraction of each segment by dividing them all by the plant transpiration:

$$\mathbf{SUF} = \frac{\mathbf{J_r}}{J_{\times l,1}} \tag{E.13}$$

References

[1] M. Javaux, V. Couvreur, J. Vanderborght, H. Vereecken, Root water uptake: from three-dimensional biophysical processes to macroscopic modeling approaches, Vadose Zone J. 12 (2013) 0, doi:10.2136/vzj2013.02.0042.

[2] J.G. Wesseling, Meerjarige simulatie van grondwaterstroming voor verschillende bodemprofielen, grondwatertrappen en gewassen met het model SWATRE, Rapport/DLO-Staring Centrum: 152, Wageningen PB - DLO-Staring Centrum SN - 0924-3070, 1991. http://edepot.wur.nl/304226.

[3] P.A.D. Musters, W. Bouten, A method for identifying optimum strategies of measuring soil water contents for calibrating a root water uptake model, J. Hydrol. 227 (2000) 273–286.

[4] F. Hupet, M. Vanclooster, Micro-variability of hydrological processes at the maize row scale: implications for soil water content measurements and evapotranspiration estimates, J. Hydrol. 303 (2005) 247–270, doi:10.1016/j.jhydrol.2004.07.017.

[5] B. Vandoorne, L. Beff, S. Lutts, M. Javaux, Root water uptake dynamics of var. Under water-limited conditions, Vadose Zone J. 11 (2012) 0, doi:10.2136/vzj2012.0005.

[6] J. Passioura, Hydraulic resistance of plants. I. constant or variable? Funct. Plant Biol. 11 (1984) 333–339.

[7] G.B. North, P.S. Nobel, Changes in hydraulic conductivity and anatomy caused by drying and rewetting roots of agave deserti (Agavaceae), Am. J. Bot. 78 (1991) 906–915, doi:10.2307/2445169.

[8] E.L. Fiscus, P.J. Kramer, General model for osmotic and pressure-induced flow in plant roots, Proc. Natl. Acad. Sci. 72 (1975) 3114–3118.

[9] J.J. Landsberg, N.D. Fowkes, Water movement through plant roots, Ann. Bot. 42 (1978) 493–508, doi:10.1093/oxfordjournals.aob.a085488.

[10] F. Meunier, V. Couvreur, X. Draye, J. Vanderborght, M. Javaux, Towards quantitative root hydraulic phenotyping: novel mathematical functions to calculate plant-scale hydraulic parameters from root system functional and structural traits, J. Math. Biol. (2017), doi:10.1007/s00285-017-1111-z.

[11] M. Biondini, Allometric scaling laws for water uptake by plant roots, J. Theor. Biol. 251 (2008) 35–59, doi:10.1016/j.jtbi.2007.11.018.

[12] T. Roose, A.C. Fowler, A model for water uptake by plant roots, J. Theor. Biol. 228 (2004) 155–171, doi:10.1016/j.jtbi.2003.12.012.

[13] D.M. Alm, J. Cavelier, P.S. Nobel, A finite-element model of radial and axial conductivities for individual roots: development and validation for two desert succulents, Ann. Bot. 69 (1992) 87–92.

[14] C. Doussan, L. Pagès, G. Vercambre, Modelling of the hydraulic architecture of root systems: an integrated approach to water absorption—model description, Ann. Bot. 81 (1998) 213–223, doi:10.1006/anbo.1997.0540.

[15] M. Zarebanadkouki, F. Meunier, V. Couvreur, J. Cesar, M. Javaux, A. Carminati, estimation of the hydraulic conductivities of lupine roots by inverse modelling of high-resolution measurements of root water uptake, Ann. Bot. (2016) mcw154, doi:10.1093/aob/mcw154.

[16] PhD thesis: Schroeder, Natalie. Three-dimensional solute transport modeling in coupled soil and plant root systems, prom.: Javaux, Mathieu, 28/08/2013. http://hdl.handle.net/2078.1/133751.

[17] M. Javaux, T. Schröder, J. Vanderborght, H. Vereecken, Use of a three-dimensional detailed modeling approach for predicting root water uptake, Vadose Zone J. 7 (2008) 1079–1088.

[18] K.J. Foster, S.J. Miklavcic, Modeling root zone effects on preferred pathways for the passive transport of ions and water in plant roots, front, Plant Sci (2016) 7, doi:10.3389/fpls.2016.00914.
[19] J. Sakurai-Ishikawa, M. Murai-Hatano, H. Hayashi, A. Ahamed, K. Fukushi, T. Matsumoto, Y. Kitagawa, Transpiration from shoots triggers diurnal changes in root aquaporin expression: transpiration triggers root aquaporin expression, Plant Cell Environ. 34 (2011) 1150–1163, doi:10.1111/j.1365-3040.2011.02313.x.
[20] M.A. Zwieniecki, M.V. Thompson, N.M. Holbrook, Understanding the hydraulics of porous pipes: tradeoffs between water uptake and root length utilization, J. Plant Growth Regul 21 (2002) 315–323, doi:10.1007/s00344-003-0008-9.
[21] K.J. Foster, S.J. Miklavcic, On the competitive uptake and transport of ions through differentiated root tissues, J. Theor. Biol. 340 (2014) 1–10, doi:10.1016/j.jtbi.2013.09.004.
[22] J. Claus, A. Bohmann, A. Chavarría-Krauser, Zinc uptake and radial transport in roots of Arabidopsis thaliana: a modelling approach to understand accumulation, Ann. Bot. 112 (2013) 369–380, doi:10.1093/aob/mcs263.
[23] E. Steudle, C.A. Peterson, How does water get through roots? J. Exp. Bot. 49 (1998) 775–788, doi:10.1093/jxb/49.322.775.
[24] V. Couvreur, M. Faget, G. Lobet, M. Javaux, F. Chaumont, X. Draye, Novel multiscale insights into the composite nature of water transport in roots,, bioRxiv (2017), doi:10.1101/147314.
[25] K.J. Foster, S.J. Miklavcic, Mathematical modelling of the uptake and transport of salt in plant roots, J. Theor. Biol. 336 (2013) 132–143, doi:10.1016/j.jtbi.2013.07.025.
[26] V. Couvreur, J. Vanderborght, M. Javaux, A simple three-dimensional macroscopic root water uptake model based on the hydraulic architecture approach, Hydrol Earth Syst Sci 16 (2012) 2957–2971.
[27] T.H. van den Honert, Water transport in plants as a catenary process, Discuss. Faraday Soc. 3 (1948) 146, doi:10.1039/df9480300146.
[28] M.N. Nimah, R.J. Hanks, Model for estimating soil water, plant, and atmospheric interrelations: I. Description and sensitivity1, Soil Sci. Soc. Am. J. 37 (1973) 522, doi:10.2136/sssaj1973.03615995003700040018x.
[29] J.-P. Lhomme, Formulation of root water uptake in a multi-layer soil-plant model: does van den Honert's equation hold? Hydrol. Earth Syst. Sci. 2 (1998) 31–39, doi:10.5194/hess-2-31-1998.
[30] G.G. Amenu, P. Kumar, A model for hydraulic redistribution incorporating coupled soil-root moisture transport, Hydrol. Earth Syst. Sci. 12 (2008) 55–74, doi:10.5194/hess-12-55-2008.
[31] C. Doussan, G. Vercambre, L. Pagès, Modelling of the hydraulic architecture of root systems: an integrated approach to water absorption—distribution of axial and radial conductances in maize, Ann. Bot. 81 (1998) 225–232.
[32] G. Lobet, L. Pagès, X. Draye, A novel image-analysis toolbox enabling quantitative analysis of root system architecture, Plant Physiol 157 (2011) 29–39.
[33] G. Lobet, X. Draye, Novel scanning procedure enabling the vectorization of entire rhizotron-grown root systems, Plant Methods 9 (2013) 1, doi:10.1186/1746-4811-9-1.
[34] L. Stingaciu, H. Schulz, A. Pohlmeier, S. Behnke, H. Zilken, M. Javaux, H Vereecken, In situ root system architecture extraction from magnetic resonance imaging for water uptake modeling, Vadose Zone J. (2013) 00, doi:10.2136/vzj2012.0019.
[35] R.J. Flavel, C.N. Guppy, M. Tighe, M. Watt, A. McNeill, I.M. Young, Non-destructive quantification of cereal roots in soil using high-resolution X-ray tomography, J. Exp. Bot. 63 (2012) 2503–2511, doi:10.1093/jxb/err421.
[36] N. Koebernick, K. Huber, E. Kerkhofs, J. Vanderborght, M. Javaux, H. Vereecken, D. Vetterlein, Unraveling the hydrodynamics of split root water uptake experiments using CT scanned root architectures and three dimensional flow simulations, Front, Plant Sci. 6 (2015), doi:10.3389/fpls.2015.00370.
[37] F. Somma, J.W. Hopmans, V. Clausnitzer, Transient three-dimensional modeling of soil water and solute transport with simultaneous root growth, root water and nutrient uptake, Plant Soil 202 (1998) 281–293.
[38] L. Pagès, G. Vercambre, J.L. Drouet, F. Lecompte, C. Collet, J. Le Bot, Root Typ: a generic model to depict and analyse the root system architecture, Plant Soil. 258 (2004) 103–119.
[39] V. Couvreur, J. Vanderborght, L. Beff, M. Javaux, Horizontal soil water potential heterogeneity: simplifying approaches for crop water dynamics models, Hydrol. Earth Syst. Sci. 18 (2014) 1723–1743, doi:10.5194/hess-18-1723-2014.
[40] N. Schröder, N. Lazarovitch, J. Vanderborght, H. Vereecken, M. Javaux, Linking transpiration reduction to rhizosphere salinity using a 3D coupled soil-plant model, Plant Soil 377 (2014) 277–293, doi:10.1007/s11104-013-1990-8.
[41] G. Lobet, M.P. Pound, J. Diener, C. Pradal, X. Draye, C. Godin, M. Javaux, D. Leitner, F. Meunier, P. Nacry, T.P. Pridmore, A. Schnepf, Root system markup language: toward a unified root architecture description language, Plant Physiol. (2015) 114.253625, doi:10.1104/pp.114.253625.
[42] J. Sanderson, F.C. Whitbread, D.T. Clarkson, Persistent xylem cross-walls reduce the axial hydraulic conductivity in the apical 20 cm of barley seminal root axes: implications for the driving force for water movement, Plant Cell Environ. 11 (1988) 247–256.
[43] J. Frensch, E. Steudle, Axial and radial hydraulic resistance to roots of maize (Zea mays L.), Plant Physiol. 91 (1989) 719–726.
[44] M. Tazawa, E. Ohkuma, M. Shibasaka, S. Nakashima, Mercurial-sensitive water transport in barley roots, J. Plant Res. 110 (1997) 435–442.
[45] H. Bramley, D.W. Turner, S.D. Tyerman, et al., Water flow in the roots of crop species: the influence of root structure, aquaporin activity, and waterlogging, Adv Agron. 96 (2007) 33–196.
[46] L. Thévenin, Extension of Ohm's law to complex electromotive circuits, Ann. Télégraphiques 10 (1883) 222–224.
[47] N. Trillo, R.J. Fernández, Wheat plant hydraulic properties under prolonged experimental drought: stronger decline in root-system conductance than in leaf area, Plant Soil. 277 (2005) 277–284, doi:10.1007/s11104-005-7493-5.
[48] C. Hachez, D. Veselov, Q. Ye, H. Reinhardt, T. Knipfer, W. Fricke, F. Chaumont, Short-term control of maize cell and root water permeability through plasma membrane aquaporin isoforms: maize root plasma membrane aquaporins, Plant Cell Environ. 35 (2012) 185–198, doi:10.1111/j.1365-3040.2011.02429.x.
[49] F. Meunier, V. Couvreur, X. Draye, J. Vanderborght, M. Javaux, Water movement through plant roots: exact solutions of the water flow equation in roots with varying hydraulic properties, Hydrol. Earth Syst. Sci. Discuss. (2016) 1–35, doi:10.5194/hess-2016-633.
[50] F. Meunier, V. Couvreur, X. Draye, J. Vanderborght, M. Javaux, A new model for optimizing the water acquisition of root hydraulic architectures over full crop cycles, in: Proceedings of the IEEE International Conference on Functional-Structural Plant Growth Modeling, Simulation, Visualization and Applications (FSPMA), 2016.
[51] L.A. Richards, Capillary conduction of liquids through porous mediums, Physics 1 (1931) 318–333, doi:10.1063/1.1745010.
[52] F. Meunier, V. Couvreur, X. Draye, G. Lobet, K. Huber, N. Schröder, A. Schnepf, J. Vanderborght, H. Vereecken, M. Javaux, Investigating soil-root interactions with the numerical model R-SWMS, Plant Syst. Biol. (2017) Submitted.
[53] J.A. Postma, J.P. Lynch, Complementarity in root architecture for nutrient uptake in ancient maize/bean and maize/bean/squash polycultures, Ann. Bot. 110 (2012) 521–534, doi:10.1093/aob/mcs082.